Applied Surface Science Advances 18 (2023) 100469

Contents lists available at ScienceDirect

Applied Surface Science Advances

journal homepage: www.sciencedirect.com/journal/applied-surface-science-advances

XPS surface analysis of ceria-based materials: Experimental methods and considerations

Mark A. Isaacs [a,b,*], Charalampos Drivas [a,c,d], Roxy Lee [a,b], Robert Palgrave [a,b], Christopher M.A. Parlett [c,d], David J. Morgan [a,e]

[a] HarwellXPS, Research Complex at Harwell, Rutherford Appleton Labs, OX16 0FA, United Kingdom
[b] Department of Chemistry, University College London, 20 Gordon Street, London WC1H 0AJ, United Kingdom
[c] Department of Chemical Engineering, University of Manchester, Manchester M13 9PL, United Kingdom
[d] Catalysis Hub, Research Complex at Harwell, Rutherford Appleton Labs, OX16 0FA, United Kingdom
[e] Translational Research Hub, Cardiff University, Maindy, Cardiff CF24 4HF, United Kingdom

ARTICLE INFO

Keywords:
XPS
Cerium
Surface analysis
X-ray Reduction

ABSTRACT

X-ray photoelectron spectroscopy (XPS) analysis of cerium is ubiquitous amongst the catalytic and materials literature however errors in experimental procedure and data analysis are often easily proliferated. In this work we focus on the best practice for experimental construction when approaching the task of understanding chemical environments in cerium-based materials by XPS.

1. Introduction

Ceria is a vital catalyst within the academic and industrial catalytic spheres. Understanding of the oxygen and cerium chemistry is key to improved design of high performance catalysts [1], and as such XPS has been employed as a standard characterisation technique for the determination of cerium (III) content within a catalytic system and inference of material reducibility.

Analysis of cerium environments within materials by XPS is a challenging affair, with detailed understanding of the spectral envelopes requiring extensive peak modelling. Fortunately, there is extensive works in this area led tirelessly by Ernesto Paparazzo enabling experienced spectroscopists to peak fit cerium environments using the tools and peak models developed herein [2–7], and this work will instead focus on the experimental parameters affecting accurate data acquisition.

Cerium (IV) is known to reduce under X-ray irradiation, having first been observed by Paparazzo in 1990 [4], through the formation of a 3d core-hole and subsequent auger decay [8], photoelectron induced reduction[9], or X-ray induced localised heating [10]. It has previously been noted that ceria in the nanocrystalline form reduces at a differing rate to that when in its microcrystalline form, [11] attributed to variances in oxygen vacancy content and oxygen diffusion kinetics. Additional consideration ought be heeded in the experimental design of XPS analysis of ceria nanoparticles given the observations of Zhang et al. of the reduction via exposure to UHV envinroments [12]. Given the importance of understanding the cerium environment within materials it is crucial to ensure experimental procedures for sample analysis maintain appropriate standards, especially given the existing concerns over the data treatment procedures employed by researchers form outside of the surface science sector [2].

To that end, developing robust experimental procedures for the analysis of cerium containing materials by XPS is of crucial importance. In this work we look at several aspects of practical XPS (and associated technique) method development and investigate the ways in which the surface analysis of such materials may influence the eventual outcome.

2. Materials and methods

2.1. X-ray photoelectron spectroscopy

All analysis was performed on a ceria standard (CAS: 1306–38–3) purchased from Sigma-Aldrich (99 %, crystallite size ~33 nm from XRD – Fig. S1). Samples were mounted by pressing powders into copper tape.

Kratos XPS data was acquired using a Kratos Axis SUPRA using monochromated Al kα (1486.69 eV) X-rays at 15 mA emission and 12 kV HT (180 W – unless otherwise stated) and an analysis area of 700 × 300 μm. The instrument was calibrated to gold metal Au 4f (83.95 eV) and

* Corresponding author at: HarwellXPS, Research Complex at Harwell, Rutherford Appleton Labs, OX16 0FA, United Kingdom.
E-mail address: mark.isaacs@ucl.ac.uk (M.A. Isaacs).

https://doi.org/10.1016/j.apsadv.2023.100469
Received 9 June 2023; Received in revised form 3 October 2023; Accepted 5 October 2023
Available online 10 October 2023

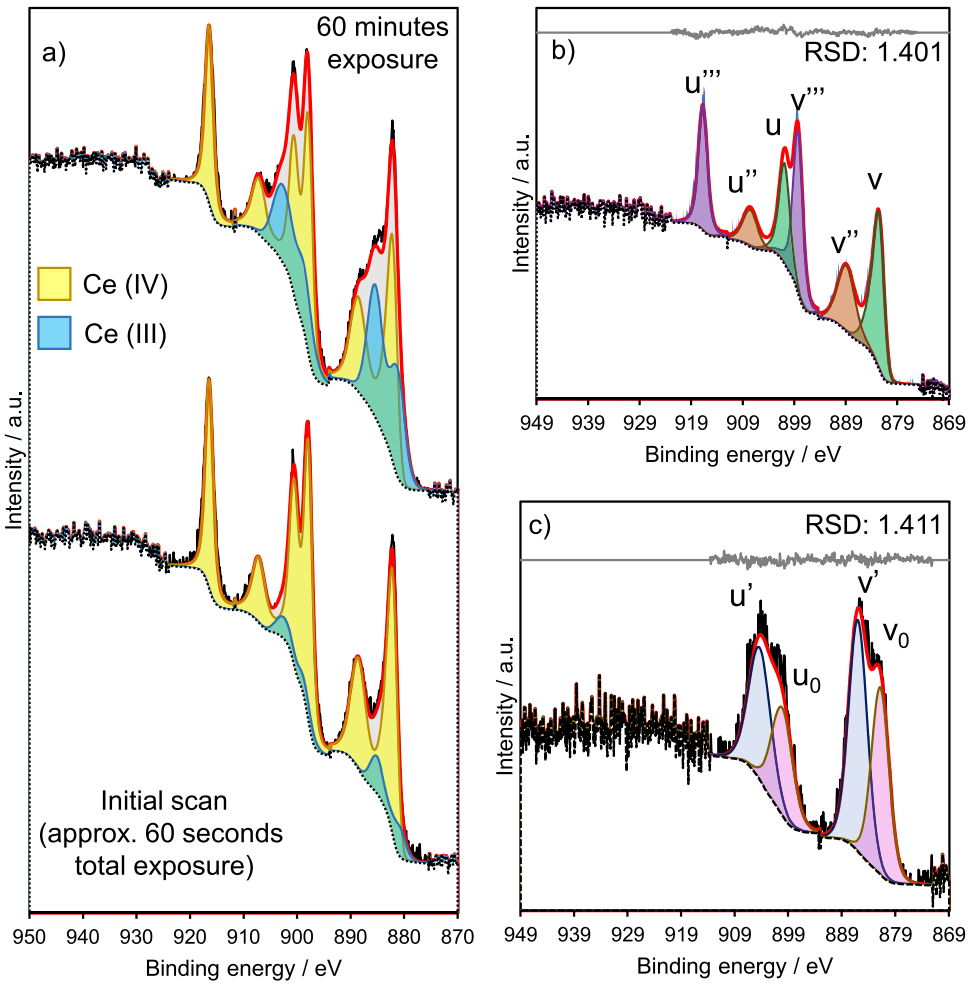

Fig. 1. (a) CeO_2 pre- and post-exposure to X-ray irradiation, (b) isolated Ce (IV) components from difference spectra and (c) isolated Ce (III) components from difference spectra run using Kratos AXIS Supra instrument.

dispersion adjusted give a BE of 932.6 eV for the Cu 2p3/2 line of metallic copper. Ag $3d_{5/2}$ line FWHM at 10 eV pass energy was 0.54 eV. Source resolution for monochromatic Al Kα X-rays is ~0.3 eV. The instrumental resolution was determined to be 0.29 eV at 10 eV pass energy using the Fermi edge of the valence band for metallic silver. Instrument resolution with charge compensation system on determined to be <1.33 eV FWHM on PTFE. Ce 3d and O 1 s high resolution spectra were obtained individually in binding energy windows of 945 – 870 eV and 540–520 eV respectively using a pass energy of 40 eV, step size of 0.1 eV and dwell time of 100 ms, resulting in a line width of ca. 0.7 eV for Au $4f_{7/2}$. Survey spectra were obtained using a pass energy of 160 eV. Charge neutralisation was achieved using an electron flood gun with filament current = 0.4 A, charge balance = 4 V, filament bias = 5 V. Successful neutralisation was adjudged by analysing the C 1 s region wherein a sharp peak with no lower BE structure was obtained. Spectra have been charge corrected to the Ce (IV) 3d u''' emission set to 916.7 eV. All data was recorded at a base pressure of below 9×10^{-9} Torr and a room temperature of 294 K.

Thermo XPS Analysis was performed using a Thermo NEXSA XPS fitted with a micro-focused monochromatic Al kα X-ray source (1486.7 eV), a spherical sector analyser and 3 multichannel resistive plate, 128 channel delay line detectors. All data was recorded at 75 W and an X-ray beam size of 400 × 200 μm. Survey scans were recorded at a pass energy of 160 eV, and high-resolution scans recorded at a pass energy of 20 eV. Electronic charge neutralization was achieved using a Dual-beam low-energy electron/ion source (Thermo Scientific FG-03). Ion gun current = 150 μA. Ion gun voltage = 45 V. All sample data was recorded at a pressure below 10^{-8} Torr and a room temperature of 294 K. Depth profiling was performed using monoatomic Argon ions at 4 kV over a 2 × 1 mm raster area.

XPS Data was analysed using CasaXPS v2.3.26rev1.0 N. Peaks were fit with a Shirley background prior to component analysis. Ce (III) and Ce (IV) envelopes were developed using a modified method from Romeo et al. and modelled using difference spectra from fresh and X-ray reduced Ce 3d spectra from commercial CeO_2 (Sigma Aldrich, 99%, CAS: 1306–38–3, ~33 nm).

ISS measurements were recorded using a Thermo NEXSA spectrometer and a 1 keV MAGCIS He^+ ion beam rastered across 1 mm^2. Spectra were recorded with a step size of 0.1 eV and a pass energy of 200 eV. Spectra were imported into CasaXPS v2.3.26rev1.0 N for quantification using a LEIS background.

Raman measurements were recorded using a confocal Thermo iXR Raman spectrometer, fitted within a Thermo NESXA XP spectrometer. Spectra were recorded using a 785 nm laser and a step size of 1 cm^{-1}. Data was analysed using OMNIC for Dispersive Raman v9.11.706.

Theoretical calculations were performed using the periodic plane-wave DFT code VASP [13], using recommended PAW potentials and the GGA functional of Perdew-Burke-Ernzehof (PBE) [14] adapted for solids (PBEsol)[15]. Geometry optimisation and electronic structure calculations were performed using GGA+*U* calculations, which were constructed by supplementing GGA theory with the Dudarev '+*U*' term [16]. This approach has been used in the literature to describe the Ce 4*f* states in CeO_2 and Ce_2O_3 [17–19]. A $U(Ce_f)$ term of 5.0 eV was used to calculate the electronic structure of CeO_2 [17].

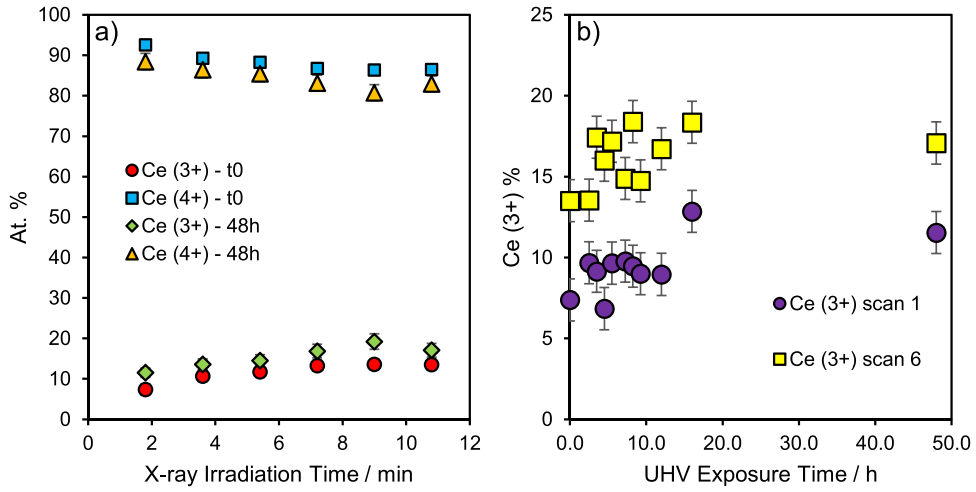

Fig. 2. Ceria oxidation state as a function of UHV exposure time.

XRD was performed using a Rigaku miniflex benchtop XRD fitted with a Cu kα source (1.54 Å), with a Ni kβ filter and a D/tex Ultra high-speed silicon strip detector. Diffractograms were recorded between 10 and 80° with a step size of 0.1° and a dwell time of 2 s.

3. Results and discussion

3.1. Cerium 3d spectra modelling

To assess cerium oxidation state and behaviour under X-ray illumination, photoelectron spectra were recorded individually as a function of illumination time under a fixed, constant X-ray flux. Established models pertaining to the peak fitting of cerium (III) and (IV) exist, accounting for the many final state effects responsible for the complex Ce 3d region and an adapted model from Romeo et al.*[3]* was used as a first pass model, with asymmetric modifiers for the *v* and *u* peaks of the Ce (IV) model LA(0.9,2,50), according to a model fit developed from a single crystal CeO_2 standard [20,21].

CasaXPS was used to obtain difference spectra from the initial scan vs a spectra following prolonged exposure (Fig. 1) and spectra representative of pure Ce^{3+} and pure Ce^{4+}, were obtained – with spectral parameters representative of the instrument in question. The difference spectra were isolated using the 'difference spectra' function within CasaXPS, and the point of divergence at the median used to identify the two phases. These spectra were fit using a non-linear least square (NLLS) approach and combined in order to describe all subsequent datasets [22,23].

3.2. Instrumental considerations for CeO_2 analysis

3.2.1. Reduction as a function of vacuum exposure

Ceria is well known to reduce over a period of time when exposed to UHV conditions [12], and as such in order to fairly assess reduction rates in the presence of additional stimulating factors – an assessment of Ce reduction as a function of vacuum exposure time (spanning the typical time period of a series of measurements) was performed in which cerium oxide (manual height adjustment in the absence of irradiating radiation) was measured at set time points following sample loading. Each measurement was performed on a fresh area of sample in order to isolate the process of vacuum reduction from that of X-ray irradiation induced induction (Fig. 2). From the measurements performed it may be concluded that the quantification of such materials be best performed within the first few hours of UHV exposure, though for the measurements procedures utilised within this work, reduction due to UHV exposure need not be considered a significant issue.

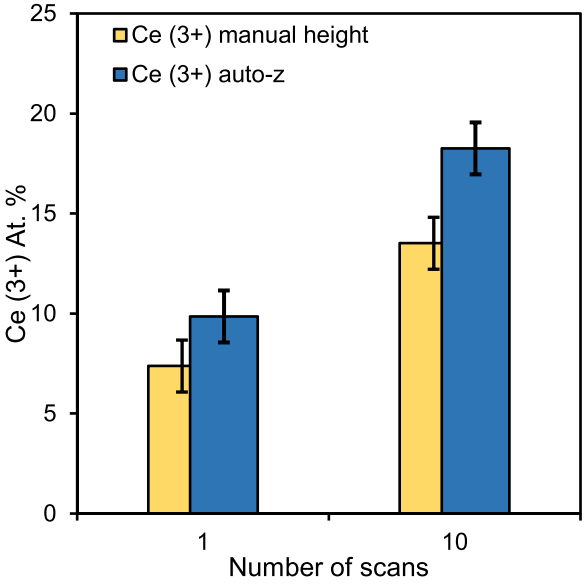

Fig. 3. Oxidation states of CeO_2 following automated vs manual sample height optimisation.

3.2.2. Sample analysis position optimisation

Typically, maximising signal intensity is achieved by finding the analysis spot for a sample (i.e. moving the sample vertically until the sample finds the cross section of the incoming X-ray beam and the analysis column). This process may be performed manually or automatically on modern spectrometers, though in the case of ceria-based samples – one ought consider optimising this parameter manually and with any X-ray illumination ceased – to prevent unwanted sample reduction prior to even a single spectral acquisition [24]. It should be noted that relying on a visual height optimisation will require good alignment between the optimal camera and the analysis position. In order to assess the degree of reduction for a standard sample (pure CeO_2); reduction profiles were recorded for samples having undergone the automated sample position process vs manual sample process (Fig. 3).

3.2.3. Reduction rates by instrument type

Instrumental factors must also be considered when performing analysis of Ce 3d XP regions, with local irradiating beam configurations resulting in significant differences in not only the initial rates of

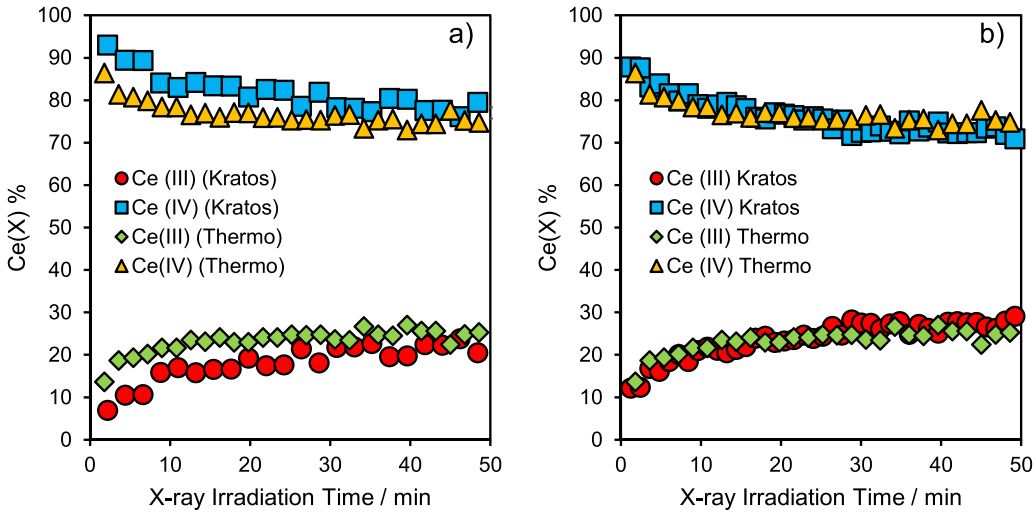

Fig. 4. Ceria reduction rates for a Kratos AXIS Supra vs Thermo NEXSA instrument under (a) standard operating conditions and (b) normalised surface radiant flux.

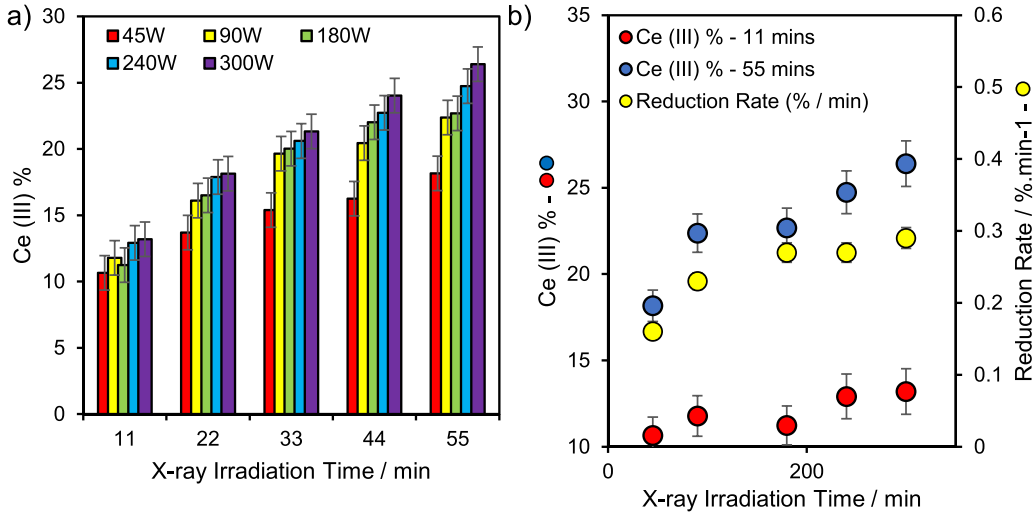

Fig. 5. Reduction behaviour of CeO_2 as a function of X-ray flux recorded using a Kratos Supra; (a) Ce(III) evolution over time and (b) minimum and maximum reductions per X-ray flux, and overall rate of reduction.

reduction, but also the ultimate plateau point after what could be considered a reasonable examination period (Fig. 4a) under standard, recommended operating conditions (Kratos – 180 W unfocused beam, Nexsa – 72 W focused beam (400 μm spot)).

This variance in reduction, using standard conditions, can be attributed largely to the difference in X-ray flux density at the sample analysis spot, since, while the Kratos beam may be at a higher power the spot size is larger (700 × 300 μm, compared with 400 × 200 μm for the Thermo instrument), and hence the surface radiant flux is higher for the Thermo instrument, compared with the Kratos (9.4 TW.m^{-2} vs 8.6 TW.m^{-2} respectively). This difference can be accounted for through control over the Kratos X-ray gun emission current and when increasing the emission current to normalise surface radiant flux, we then see more comparable reduction kinetics (Fig. 4b).

Kratos X-ray guns permit fine tuning of filament current and overall irradiative power and as such, measures may be implemented in order to counterbalance the reductive effects of X-ray irradiation through the lowering of X-ray power. Fig. 5a reports the degree of reduction following X-ray irradiation at various X-ray powers and the desirable impact of utilising a low power source may be seen in the low Ce(III) contents obtained from using a 45 W X-ray source. Furthermore, if we look at the rate of reduction as a function of power (Fig. 5b), we see that using a low power source minimises the percentage reduction per minute. If it proves possible to obtain appropriate signal:noise spectra using a low power source, it ought be concluded that this represents the preferable experimental set-up when analysing ceria-based materials. This observation should be of particular importance when considering samples analysed by high flux density sources (e.g. synchrotron radiation), in which the potential for high levels of rapid reduction exists. In such cases, the use of mitigating techniques such as ensuring ceria regions are analysed first, prior to prolonged beam exposure, may be of even higher importance.

3.2.4. *Analysis of ceria valence band during reduction*

Spectral fitting of Ce 3d is a daunting task and the complexity of the model fit has the potential to introduce errors into the system as well – hence robust data modelling must be applied when peak fitting of these systems. Valence spectra and, by extension, UPS analysis may also provide invaluable information into the chemical environment of the ceria states within the material structure. Recent work by Cardenas et al. provides guidance on using UPS as a crucial tool in understanding the surface of ceria to quantify sub-stoichiometric ceria contents with a high surface sensitivity (of particular to fields such as catalysis) [25]. While this provides a pathway towards successful chemical understanding of

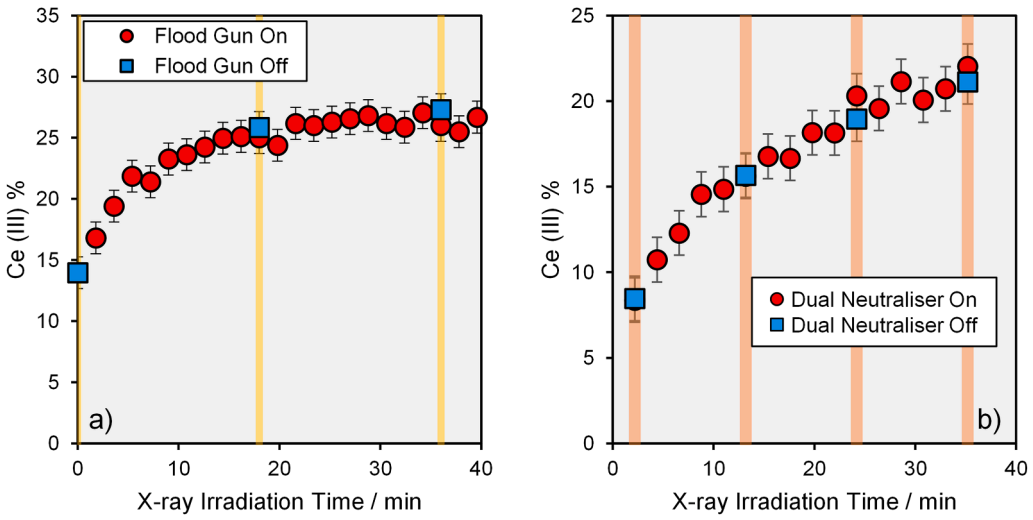

Fig. 6. Reduction profiles for CeO_2 run using (a) Kratos Supra low energy electron flood gun and (b) Thermo NEXSA dual neutraliser system in both FG on and FG off modes.

bulk ceria materials, the added complexity of the valence band when considering composites or mixed oxides results in this approach becoming a much more challenging ordeal and therefore appreciation of the Ce 3d spectra remains a vital tool in the arsenal of the spectroscopist.

The valence band is predominantly O 2p in nature and the conduction band minimum (CBM) is mainly composed of Ce 5d states, with the appearance of an empty Ce 4f state above the valence band maximum (VBM), which is consistent with other ab initio calculations [17–19]. The Ce 4f state that lies within the O 2p – Ce 5d band gap in CeO_2 is unoccupied, whereas in the Ce_2O_3 analogue, the Ce 4f state is closer to the O 2p VB and is occupied [18]. A comparison of the calculated DOS for CeO_2 and VB XPS in Fig. S2. The Ce 4f peak may become populated on conversion to Ce^{3+} and can be attributed to the presence of Ce^{3+} ions in partially reduced ceria surfaces [17]. Mullins et al. have assigned the low BE feature to Ce 4f by comparing soft XPS (300 – 530 eV) VB spectra of reduced cerium oxide films of varying compositions [26]. Henderson et al. similarly attribute the appearance of a peak near the leading edge of the CeO_2 VB to Ce 4f in Ce^{3+} species in sub stoichiometric ceria surfaces [27].

In order to verify the reduction of these systems and the Ce 3d peak fitting models used – analysis of the valence band was undertaken using Al kα X-rays (Thermo NEXSA) and modelled using DFT (Fig. S2). We see an appreciable increase in the Ce 4f population at ~ 1.2 eV, providing additional confirmation of the presence of substoichiometric ceria following X-ray reduction.

3.2.5. *Usage of charge neutraliser system*

Dual neutralisation systems utilise low energy ion beams alongside an electron beam, deemed of little hazard to the vast majority of standards. Nevertheless, particularly sensitive samples have indeed been shown to suffer degradation from prolonged exposure [28], though particular experimental considerations may in fact reduce the severity of this greatly [29]. While higher energy ions are well known to disrupt CeO_2 structures, converting them to Ce_2O_3 [30,31], and even relatively low energy Ar^+ ions [32], the effect of these low energy ion neutralisers has not yet been evaluated.

CeO_2 samples were measured in snapshots with both the flood gun on and off (Fig. 6) – though in the case of flood gun off, periodic spectra were obtained with the flood gun on in order to combat sample charging and enable quantification of the spectra. In both the cases of the low energy electron flood gun (Kratos Supra) and dual electron/Ar^+ neutraliser (Thermo NEXSA) the use of the flood gun did not appear to exacerbate or hinder the degree of reduction from X-ray exposure alone.

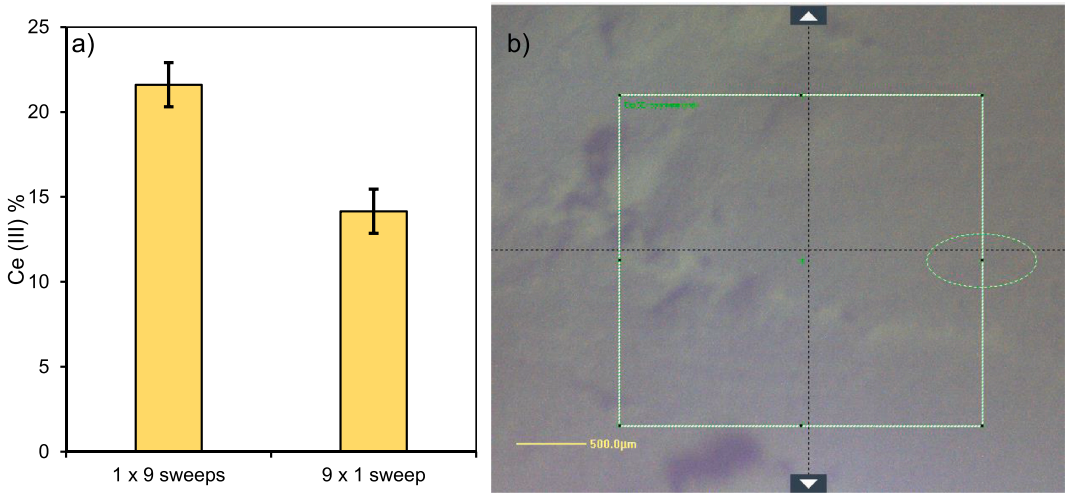

Fig. 7. (a) quantification of Ce(III) of CeO_2 following 9 sweeps on a single analysis spot vs cumulative spectral addition of 1 sweep of 9 analysis spots and (b) Thermo NEXSA multiple area scan tool.

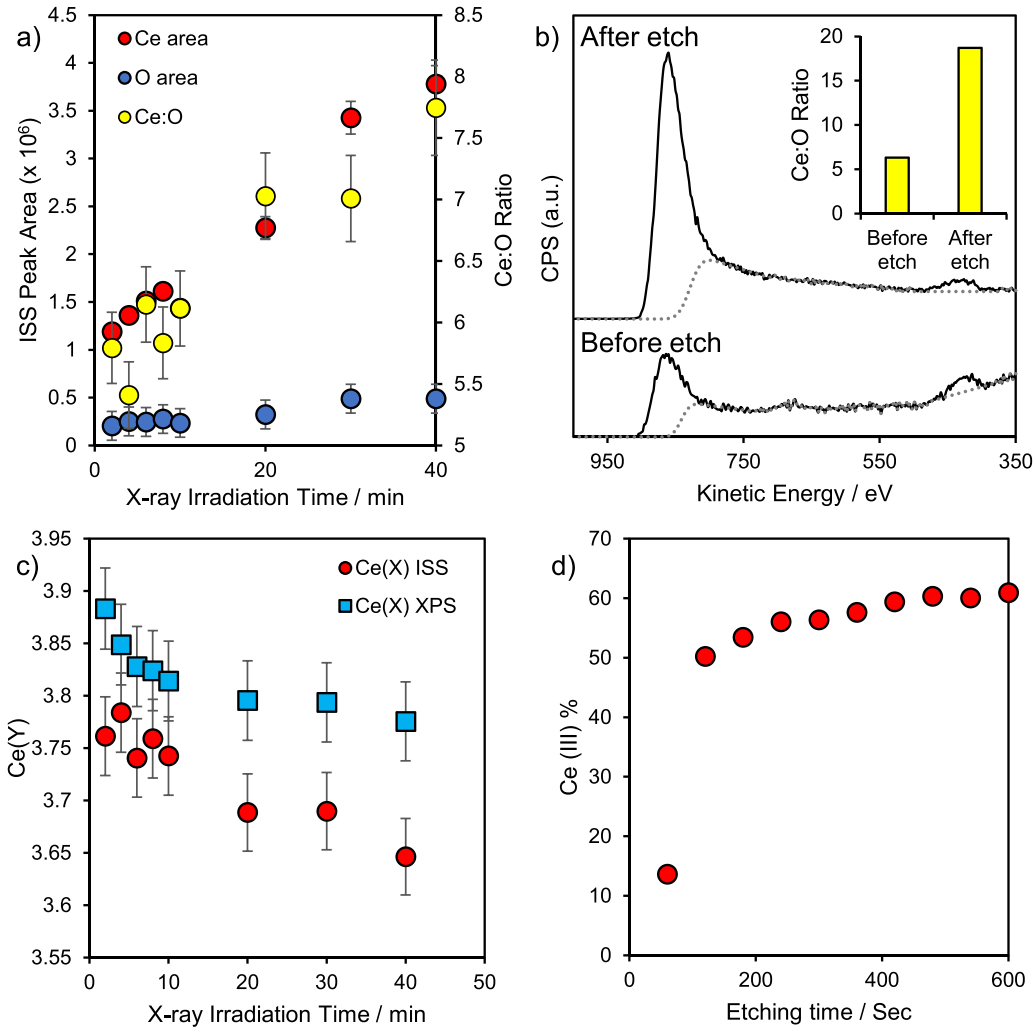

Fig. 8. (a) ISS peak area ratios as a function of total X-ray exposure time, (b) ISS spectra of fresh and Ar^+ etched CeO_2, (c) calculated average cerium oxidation state (Y) as a function of total X-ray exposure and (d) Ce(III) content as a function of Ar^+ ion beam irradiation time.

3.2.6. Sample imaging tools

Modern spectrometers are often equipped with easy-to-use tools for rapid access of samples across a pre-defined area. One of the benefits of this is the facile construction of an experimental method by which to analyse a single sweep of an analysis spot, for X number of spots across an area of Y x Z mm. This may provide a considerable advantage when analysing samples with low ceria content which may require a high number of sweeps to obtain appropriate signal:noise for accurate modelling. An example of this may be found in Fig. 7, whereby the Thermo NEXSA multiple analysis spot tool was used to record 9 spectral sweeps on a single analysis spot and compared with the quantification from a merged spectra of a single sweep from 9 analysis spots. A significant difference may be observed in the Ce(III) content between the two methods, highlighting the importance of considering sample damage when measuring these systems for a prolonged period. It should be noted that in order for this technique to be used, a homogeneous sample is required with a relatively large area – enabling enough analysis space to accommodate multiple analysis spots.

3.3. Coincident raman and ion scattering spectroscopies

Ion scattering spectroscopy (ISS) reveals sample information at the very surface/near-surface of a materials and, while it may lack the detailed chemical specificity of XPS, may provide invaluable insights into the elemental composition of a sample at the crucial interface between the solid state and the atmosphere. Here, ISS was utilised to monitor changing O:Ce ratios as a function of X-ray exposure (Fig. 8).

A semi-quantified analysis of the ISS peaks was performed by obtaining an ISS measurement on a pristine CeO_2 sample (t0) and a CeO_2 powder following an extensive monotomic Ar treatment. The process of performing ISS does also reduce the CeO_2 (Fig. S3) and as such a subsequent surface analysis by XPS was performed following a single ISS sweep to determine the t0 Ce(Y) value and was determined to be ($Y = 3.75$). Given the plateau following Ar^+ etching (Fig. 8d) it was assumed that the surface of the ceria ought be entirely reduced to the Ce_2O_3 form [33] and the ISS Ce:O peak ratio (Fig. 8b) following etching was taken as the Ce^{Y+} oxide ($Y = 3$) value. Assuming a linear relationship between peak area and surface atom population, a y=mx+c correlation (Fig. S4) was then used to back calculate the average cerium oxidation state following period X-ray irradiation times (Fig. 8c) from the Ce:O peak area ratios (Fig. 8a). This was compared against the XPS quantification of the X-ray irradiated ceria (Fig. 8c) and it was observed that there appears to be a subtle difference in Ce:O between the near-surface (XPS) and upper surface (ISS) indicating that there be limited oxygen diffusion to the surface across the timeframes and size domains involved, with the upper surface reducing to a greater degree than the near-surface. This observation is consistent with previously reported data indicating the depth of X-ray induced damage occurs within the top 10–20 Å of a material surface [8].

Recent advances in instrumental design and configuration permit the

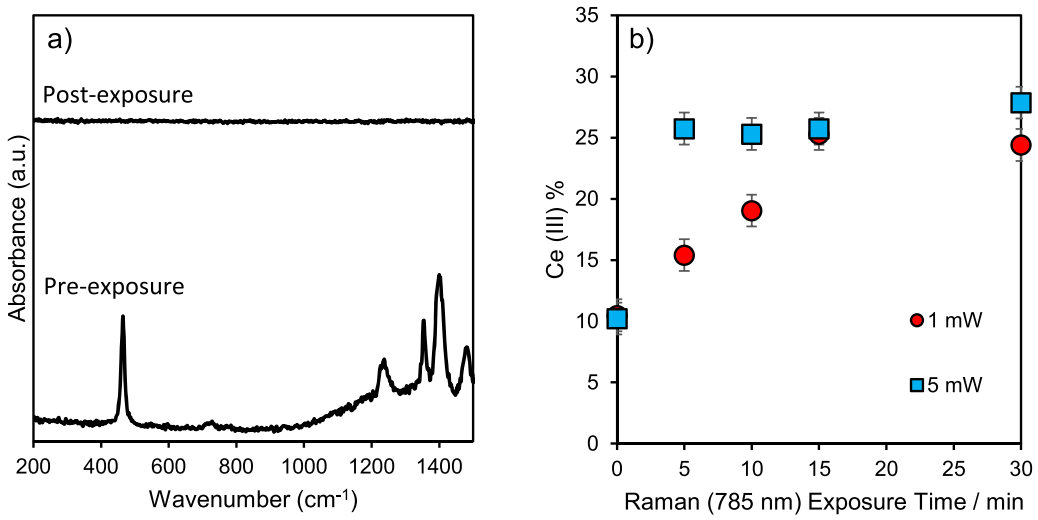

Fig. 9. (a) Raman spectra of CeO_2 before and after exposure to 30 mins 5 mW 785 nm laser irradiation in UHV conditions and (b) XPS quantification of the reduction of Raman as a function of time exposed CeO_2 in UHV conditions.

recording of coincident Raman analysis with XPS, enabling an additional dimension of information into the structural and chemical compositions of materials samples. Raman spectroscopy is traditionally performed in ambient conditions, and ceria is known to be stable under these analysis conditions. In an attempt to monitor structural changes upon exposure to X-rays, coincident Raman was performed where it was discovered that the Raman lasers would reduce the Ce(IV) sites at a far greater rate than any X-ray exposure (Fig. 9a). The rate of reduction was such that it became very challenging to obtain any meaningful Raman (whilst also obtaining Raman spectra of sufficient signal:noise), however by tuning the Raman power it became apparent that we may actually find Raman lasers a useful tool in probing relative reduction rates across ceria samples given we obtain a linear initial rate across 15 min of total exposure.

4. Conclusions

This work has highlighted the importance of care and consideration when not only analysing the data outputs from experimental analysis of cerium based systems by XPS and associated surface analysis techniques, but also in the experimental design of said measurements. X-ray power, sample alignment, UHV exposure and the use of ancillary techniques such as ion scattering and Raman spectroscopies have all been evidenced to impact the surface chemistry of ceria systems. It may be considered a useful tool for the experimental spectroscopist to follow a set of guidelines when handling ceria based materials.

1. Samples ought be analysed within the first few hours of introduction to a vacuum chamber. This might mean not taking advantage of modern instruments capacity for large batches of samples and instead recording each material as a separate experiment.
2. Take care when determining sample position. If using instrument ‘auto-z’ features to determine sample height, consider performing this on a separate spot at the same dimensional plane and then recording the spectra at a ‘fresh’ point.
3. Determine which X-ray power is suitable (if applicable). For ceria-heavy systems with a large signal:noise, using low powered X-ray sources will minimise sample degradation.
4. For low ceria content samples, consider using instrument imaging tools to record single scans of multiple areas and aggregate them post-analysis. This will ensure minimal degradation without sacrificing signal intensity.
5. Take care when using ancillary techniques, record XPS before (on a separate area) and after (on the analysis area) to determine the impact of your chosen technique on surface chemistry.

Combining this toolkit with the appropriate data handling methods will ensure you minimise potential errors in your analysis which may potentially lead to inaccurate conclusions when considering structure-function relationships in ceria based systems.

Declaration of Competing Interest

The authors declare that they have no known competing financial interests or personal relationships that could have appeared to influence the work reported in this paper.

Data availability

Data will be made available on request.

Acknowledgments

The X-ray photoelectron (XPS) data collection was performed at the EPSRC National Facility for XPS (“HarwellXPS”), operated by Cardiff University and UCL, under Contract No. PR16195. UK Catalysis Hub is kindly thanked for resources and support provided via our membership of the UK Catalysis Hub Consortium and funded by EPSRC grant: EP/R026815/1. We would like to thank Gavin Stenning for help on the Rigaku Miniflex benchtop XRD instrument in the Materials Characterisation Laboratory at the ISIS Neutron and Muon Source. R.L. acknowledges funding from the EPSRC M3S CDT (EP/L015862/1) and sponsorship by Thermo Fisher Scientific. The authors acknowledge the use of the UCL Myriad, Kathleen, and Thomas High Performance Computing Facilities (Myriad@UCL, Kathleen@UCL, Thomas@UCL), and associated support services, in the completion of this work.

Supplementary materials

Supplementary material associated with this article can be found, in the online version, at doi:10.1016/j.apsadv.2023.100469.

References

[1] G.B. Della Mea, L.P. Matte, A.S. Thill, F.O. Lobato, E.V. Benvenutti, L.T. Arenas, A. Jürgensen, R. Hergenröder, F. Poletto, F. Bernardi, Tuning the oxygen vacancy population of cerium oxide (CeO2−x, 0<x<0.5) nanoparticles, Appl. Surf. Sci. 422 (2017) 1102–1112.

[2] E. Paparazzo, XPS quantification of oxygen vacancies in mesoporous and non-mesoporous CeO2: comment on an article by Thill et al, J. Mater. Chem. A 8 (2020) 24752–24762.

[3] M. Romeo, K. Bak, J. El Fallah, F.Le Normand, L. Hilaire, XPS Study of the reduction of cerium dioxide, Surf. Interface Anal. 20 (1993) 508–512.

[4] E. Paparazzo, XPS studies of damage induced by X-ray irradiation on CeO2 surfaces, Surf. Sci. 234 (1990) L253–L258.

[5] E. Paparazzo, On the curve-fitting of XPS Ce(3d) spectra of cerium oxides, Mater. Res. Bull. 46 (2011) 323–326.

[6] E. Paparazzo, Letter to the editor, Catal. Today 185 (2012) 319–321.

[7] E. Paparazzo, Use and mis-use of x-ray photoemission spectroscopy Ce3d spectra of Ce2O3 and CeO2, J. Phys. Condens. Matter 30 (2018), 343003.

[8] E. Paparazzo, G.M. Ingo, N. Zacchetti, X-ray induced reduction effects at CeO2 surfaces: an x-ray photoelectron spectroscopy study, J. Vac. Sci. Technol. A 9 (1991) 1416–1420.

[9] D.E. Ramaker, C.T. White, J.S. Murday, Summary Abstract: auger induced desorption of covalent and ionic systems, J. Vac. Sci. Technol. 18 (1981) 748–749.

[10] E. Paparazzo, G.M. Ingo, On the X-ray induced chemical reduction of CeO2 as seen with X-ray photoemission spectroscopy, J. Electron Spectrosc. Relat. Phenom. 95 (1998) 301–304.

[11] L. Qiu, F. Liu, L. Zhao, Y. Ma, J. Yao, Comparative XPS study of surface reduction for nanocrystalline and microcrystalline ceria powder, Appl. Surf. Sci. 252 (2006) 4931–4935.

[12] F. Zhang, P. Wang, J. Koberstein, S. Khalid, S.W. Chan, Cerium oxidation state in ceria nanoparticles studied with X-ray photoelectron spectroscopy and absorption near edge spectroscopy, Surf. Sci. 563 (2004) 74–82.

[13] G. Kresse, J. Furthmuller, Efficient iterative schemes for ab initio total-energy calculations using a plane-wave basis set, Phys. Rev. B 54 (1996) 11169–11186.

[14] J.P. Perdew, K. Burke, M. Ernzerhof, Generalized gradient approximation made simple, Phys. Rev. Lett. 77 (1996) 3865–3868.

[15] J.P. Perdew, A. Ruzsinszky, G.I. Csonka, O.A. Vydrov, G.E. Scuseria, L. A. Constantin, X. Zhou, K. Burke, Restoring the density-gradient expansion for exchange in solids and surfaces, Phys. Rev. Lett. 100 (2008), 136406.

[16] S.L. Dudarev, G.A. Botton, S.Y. Savrasov, C.J. Humphreys, A.P. Sutton, Electron-energy-loss spectra and the structural stability of nickel oxide: an LSDA+U study, Phys. Rev. B 57 (1998) 1505–1509.

[17] B.J. Morgan, D.O. Scanlon, G.W. Watson, The Use of the "+*U*" correction in describing defect states at metal oxide surfaces: oxygen vacancies on $CeO_2$and TiO_2, and Li-doping of MgO, E-J. Surf. Sci. Nanotechnol. 7 (2009) 389–394.

[18] C. Loschen, J. Carrasco, K.M. Neyman, F. Illas, First-principles LDA+U and GGA+U study of cerium oxides: dependence on the effective U parameter, Phys. Rev. B 75 (2007), 035115.

[19] J.L.F. Da Silva, M.V. Ganduglia-Pirovano, J. Sauer, V. Bayer, G. Kresse, Hybrid functionals applied to rare-earth oxides: the example of ceria, Phys. Rev. B 75 (2007), 045121.

[20] T. Skála, F. Šutara, K.C. Prince, V. Matolín, Cerium oxide stoichiometry alteration via Sn deposition: influence of temperature, J. Electron Spectrosc. Relat. Phenom. 169 (2009) 20–25.

[21] D.J. Morgan, Photoelectron spectroscopy of ceria: reduction, quantification and the myth of the vacancy peak in XPS analysis, Surf. Interface Anal. 55 (2023) 845–850.

[22] T.G. Avval, N. Gallagher, D. Morgan, P. Bargiela, N. Fairley, V. Fernandez, M. R. Linford, Practical guide on chemometrics/informatics in x-ray photoelectron spectroscopy (XPS). I. Introduction to methods useful for large or complex datasets, J. Vac. Sci. Technol. A 40 (2022).

[23] T.G. Avval, H. Haack, N. Gallagher, D. Morgan, P. Bargiela, N. Fairley, V. Fernandez, M.R. Linford, Practical guide on chemometrics/informatics in x-ray photoelectron spectroscopy (XPS). II. Example applications of multiple methods to the degradation of cellulose and tartaric acid, J. Vac. Sci. Technol. A 40 (2022).

[24] BS ISO 18554:2016, Surface chemical analysis —Electron spectroscopies —Procedures for identifying,estimating and correcting for unintended degradation by X-rays in a material undergoing analysis by X-ray photoelectron spectroscopy, Br. Stand. Inst. 1 (2016) 1–17.

[25] L. Cardenas, C. Molinet-Chinaglia, S. Loridant, Unraveling Ce 3+ detection at the surface of ceria nanopowders by UPS analysis, Phys. Chem. Chem. Phys. 24 (2022) 22815–22822.

[26] D.R. Mullins, P.V. Radulovic, S.H. Overbury, Ordered cerium oxide thin films grown on Ru(0001) and Ni(111), Surf. Sci. 429 (1999) 186–198.

[27] M.A. Henderson, C.L. Perkins, M.H. Engelhard, S. Thevuthasan, C.H.F. Peden, Redox properties of water on the oxidized and reduced surfaces of CeO2(111), Surf. Sci. 526 (2003) 1–18.

[28] D.J. Morgan, XPS insights: sample degradation in X-ray photoelectron spectroscopy, Surf. Interface Anal. 55 (2023) 331–335.

[29] L. Edwards, P. Mack, D.J. Morgan, Recent advances in dual mode charge compensation for XPS analysis, Surf. Interface Anal. 51 (2019) 925–933.

[30] K.I. Maslakov, Y.A. Teterin, A.J. Popel, A.Y. Teterin, K.E. Ivanov, S.N. Kalmykov, V. G. Petrov, P.K. Petrov, I. Farnan, XPS study of ion irradiated and unirradiated CeO2 bulk and thin film samples, Appl. Surf. Sci. 448 (2018) 154–162.

[31] A. Kumar, R. Devanathan, V. Shutthanandan, S.V.N.T. Kuchibhatla, A.S. Karakoti, Y. Yong, S. Thevuthasan, S. Seal, Radiation-Induced Reduction of Ceria in Single and Polycrystalline Thin Films, J. Phys. Chem. C 116 (2012) 361–366.

[32] G.D. Wang, D.D. Kong, Y.H. Pan, H.B. Pan, J.F. Zhu, Low energy Ar-ion bombardment effects on the CeO 2 surface, Appl. Surf. Sci. 258 (2012) 2057–2061.

[33] L. Cardenas, C. Molinet-Chinaglia, S. Loridant, Unraveling Ce3+ detection at the surface of ceria nanopowders by UPS analysis, Phys. Chem. Chem. Phys. 24 (2022) 22815–22822.